34th Annual International Conference of the IEEE EMBS
San Diego, California USA, 28 August - 1 September, 2012

Probability Density Based Gradient Projection Method for Inverse Kinematics of a Robotic Human Body Model

Derek Lura, Matthew Wernke, Redwan Alqasemi, Stephanie Carey, Rajiv Dubey, *Member, IEEE*

***Abstract*—This paper presents the probability density based gradient projection (GP) of the null space of the Jacobian for a 25 degree of freedom bilateral robotic human body model (RHBM). This method was used to predict the inverse kinematics of the RHBM and maximize the similarity between predicted inverse kinematic poses and recorded data of 10 subjects performing activities of daily living. The density function was created for discrete increments of the workspace. The number of increments in each direction (x, y, and z) was varied from 1 to 20. Performance of the method was evaluated by finding the root mean squared (RMS) of the difference between the predicted joint angles relative to the joint angles recorded from motion capture. The amount of data included in the creation of the probability density function was varied from 1 to 10 subjects, creating sets of for subjects included and excluded from the density function. The performance of the GP method for subjects included and excluded from the density function was evaluated to test the robustness of the method. Accuracy of the GP method varied with amount of incremental division of the workspace, increasing the number of increments decreased the RMS error of the method, with the error of average RMS error of included subjects ranging from 7.7° to 3.7°. However increasing the number of increments also decreased the robustness of the method.**

I. Introduction

This research was completed as part of the "Development of a Simulation Tool for Upper Extremity Prostheses" at the University of South Florida. It was part of an effort to develop an accurate prediction of upper body human motion for rehabilitation and use in the design and analysis of prostheses. Previous work has shown possible secondary injury of upper body prostheses users due to compensatory motions required to overcome the limited range of motion of the prosthetic arm [1]. Studies have shown that a simulation using a simplified model of the upper body can predict possible compensatory motions [2]. Prediction and modeling of human motion has been studied in a variety of fields, including 3D graphics, human engineering, biomechanics, and others. The ability of a model to accurately predict general human motion of the upper body remains a difficult task. The use of the Jacobian for inverse kinematics control of redundant manipulators has been well studied [3-6], and the weighted least norm solution has been used in simulating movement of the human upper body [2, 7, 8]. The accuracy of the probability density based gradient projection GP method for reconstructing human motion relative to collected motion analysis data was analyzed. The accuracy of motion reconstruction using the least norm (LN) solution is also presented as a reference. A functional joint center method for segment definitions from the motion analysis data and subject specific parameters allow the RHBM to nearly perfectly reconstruct subject motion using the recorded joint angles.

Karim Abdel-Malek, Zan Mi, et al. [9, 10] have created a an upper body model and controlled its pose by optimizing a cost function, and have compared their results to motion data from the University of Michigan human motion simulation (HUMOSIM) database. However, the segments of their model and the model used in the database are not the same and only a visual comparison between the two motions is provided. Other studies have predicted upper-limb motion but with the arm originating at the glenohumeral (shoulder) joint [11-14]. These models cannot predict compensatory motions since they do not include proximal joints of the upper body.

II. Motion Capture

Ten healthy adult subjects participated in this study. Subject demographics are given in TABLE I. Motion data were collected using an eight camera Vicon® (Oxford, UK) motion analysis system with 21 passive reflective markers placed on the subject's skin with double sided adhesive tape. Range of motion (RoM) tasks and activities of daily living (ADL) of ten healthy adult male subjects were collected. For this study, the tasks of opening a door, drinking from a cup, brushing hair, lifting a laundry basket, and eating with a knife and fork were selected for the analysis. All procedures were approved by the University of South Florida Institutional Review Board, and informed consent was obtained prior to data collection.

TABLE I. Subject Demographics

Subject	Age (years)	Sex	Height (cm)	Body Mass (kg)	Dominant Hand
C01	21	M	173	62.5	R
C02	25	M	180	79.8	R
C03	20	M	181	83.5	L
C04	20	M	180	70.5	R
C05	24	M	186	100.5	R
C06	35	M	184	102.5	L
C07	38	F	160	62	R
C08	41	M	177	73.2	R
C09	58	M	174	90.5	R
C10	54	F	166	65	R
Avg (±S.D.)	**34 (±14)**	**-**	**176 (±8)**	**79 (±15)**	**-**

This research and development project was conducted by University of South Florida and is made possible by a research grant that was awarded and administered by the U.S. Army Medical Research & Materiel Command (USAMRMC) and the Telemedicine & Advanced Technology Research Center (TATRC), at Fort Detrick, MD, under Contract Number: W81XWH-10-1-0601.The views, opinions and/or findings contained in this publication are those of the authors and do not necessarily reflect the views of the Department of Defense and should not be construed as an official DoD/Army position, policy or decision unless so designated by other documentation. No official endorsement should be made.

D. J. Lura, M. M. Wernke, S. L. Carey, R. Alqasemi, and R. V. Dubey are with the Center for Assistive, Rehabilitation & Robotics Technologies (CARRT) at the Mechanical Engineering Department of the University of South Florida, Tampa, FL, 33620 USA (email: dlura@mail.usf.edu, phone: 813-974-9651).

The range of motion data were collected to find the functional joint centers of the subject's body using the methods described by Schönauer [15], and with sufficient data to satisfy the validation for use in the upper body based on previous work [16]. The model divides the upper body into segments for the pelvis, torso, shoulders (scapulae & clavicle), upper arms, forearms, and hands. Each segment was tracked by a set of markers. The pelvis was used to define the base frame and was defined by markers on the skin near the anterior, posterior, left, and right superior iliac spine of the pelvis (LASI, RASI, LPSI, and RPSI). The torso was tracked by markers on the jugular notch (CLAV) and 1st thoracic vertebrae (T1). The scapula was tracked by markers on the anterior and poster end of the acromion process (R&LSHOA, and R&LSHOP). The upper arm was tracked by the lateral and medial epicondyle of the elbow (R&LELB, and R&LELBM). The forearm was tracked by the radial and ulnar protrusion of the wrist (R&LWRA, and R&LWRB). Finally, the hand was tracked by a maker on the dorsal side of the third metacarpal head (R&LFIN). Raw marker position data were collected at 120 Hz and were filtered using an 11 point weighted moving average filter to remove noise, prior to calculation of the joint centers and joint angles.

Each task was completed three times to ensure that there was redundancy in the motion data for each subject. Each of the three trials collected were used in testing and training the algorithms. The RoM tasks were used to accurately calculate the functional joint centers, and generate the subject kinematics. The tasks require the subject to move from a neutral position to both limits of their comfortable range of motion and then return to neutral position. Details on the process of joint center extraction and segment definition have been reported [17].

III. Model Kinematics

It is important when modeling a physical system that the model and the system be coupled as closely as possible. The model was built from the data collected during the RoM tasks. The locations of each joint center, coupled with the degrees of freedom of each joint are used to calculate the Denavit and Hartenburg parameters of the upper body in the notation described by Craig [18]. Each subject has a specific set of parameters which consists of the segment lengths and joint center locations. These sets of parameters were extracted from the RoM data that were used to create the robotic model, define segments, and calculate the joint angles of the ADL tasks. By using the motion analysis data to build the model, the kinematics of the model are nearly exactly the same as kinematic chain composed from the segments from motion analysis of the subjects performing the tasks. The error of the forward kinematics of the model relative to the recorded end effector position using this method has been shown to be very small, with the average error being less than 1mm [17]. Manual measurements of subject anaotomy can also be correlated to the subject parameters if motion analysis data is not avalaible, but the forward kinematics will be slightly less accurate. The flow of data in validating the performance of this method is presented in Figure 1.

Figure 1. Flow of motion data for this study. RoM data were used to find subject kinematics, while ADL data were used for training and testing the inverse kinematics of the GP method.

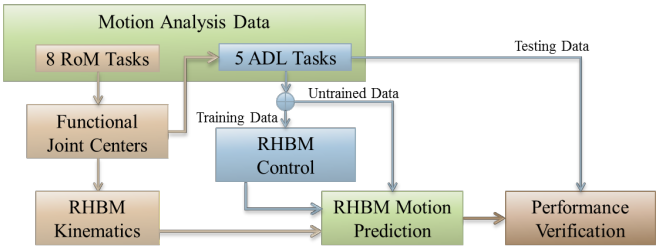

IV. Methods

This study used the bilateral end effector position to calculate the joint angles of the RHBM. The LN solution was used as a reference method to find a baseline of error. Both the LN and GP methods required calculation of the inverse of the manipulator Jacobian. For the RHBM, x is a 12 by 1 vector containing the Cartesian position and orientation of the right and left end effectors respectively, and θ represents the 1 by 25 joint angles vector. The Cartesian and joint angle velocity are presented as $\dot{x}$ and $\dot{\theta}$ respectively. The first three joints of the right and left model were represented by the torso. Composition of the bilateral Jacobian (J) from the Jacobians of the right (J_R) and left (J_L) arms, and the forward kinematics equation is given in Eq. 1. The inverse kinematics equation as described by the pseudo inverse of the Jacobian is given in Eq. 2, where (J^+) is the pseudo inverse [5]. The first three joints of the right and left arms represented the movement of the torso and were shared by both arms.

$$\dot{x} = \begin{bmatrix} \dot{x}_R \\ \dot{x}_L \end{bmatrix} = J\dot{\theta} = \begin{bmatrix} J_{R1-3} & J_{R4-14} & 0 \\ J_{L1-3} & 0 & J_{L4-14} \end{bmatrix} \begin{bmatrix} \dot{\theta}_{R\&L1-3} \\ \dot{\theta}_R \\ \dot{\theta}_L \end{bmatrix} \quad (1)$$

The least norm method uses the pseudo inverse of the Jacobian to find the mapping between end effector Cartesian and joint angle velocities; this was used to find the inverse kinematics by finding the difference between the forward kinematic solution and the desired end effector position.

$$\dot{\theta} = J^+\dot{x} \quad (2)$$

In this formulation both arms can move simultaneously but the movements of the arms were coupled. If the left hand moves and the right hand remains still, the joint angles of the right arm will have to change as well to accommodate the movement of the torso. Given a series of end effector positions and orientations, the corresponding joint angles were calculated by solving for each step in the series. Due to the non-linearity of the equations, error was introduced based on the size of the step between end effector trajectory points. In this application, this error was small because data were collected at a 120Hz frame rate and movement during the ADLs was generally slow. However, error was minimized by using the forward kinematics of the current position at each iteration when calculating the end effector difference. The formula for the iterative least norm solution is given in Eq. (3), where $fkine(\theta_i)$ is the forward kinematic solution of the RHBM.

$$\theta_{i+1} = \theta_i + J^+(x_{i+1} - fkine(\theta_i)) \quad (3)$$

This method is referred to as the least norm solution because it produces the solution to the inverse kinematics that minimizes the norm or the joint angular velocities. The gradient projection method used the null-space of the Jacobian to optimize the redundancy of the system. The joint angle velocity of the gradient projection method ($\dot{\Theta}_{GPM}$), is described in Eq. 4, and is a function of the Jacobian, the end effectors' velocity, and the gradient vector (∇H). The gradient vector ∇H is described by the gradient of a function of the joint angles that should be minimized.

$$\dot{\Theta}_{GPM} = J^{+} * \dot{x} + (I - J^{+}J) * \nabla H \qquad (4)$$

In this study, the performance was defined by the ability to reproduce the pose of the RHBM to match the pose of the subjects performing the recorded tasks. Therefore, the inverse of the joint angle density function, obtained from the motion data, was used to find the gradient vector as shown in Eq. 5. Here the gradient vector is formed by taking the partial derivatives of the inverse of the joint angle density function for each of the joint angles. The probability density function is the non-parametric density distribution as calculated by the Matlab function '*ksdensity.m*' using the joint angle data from motion analysis of subjects included in the training set. The scalar quantity k was used to affect the rate of convergence of the solution on the inverse density function. This is similar to the methods used by Artemiadis et al [13] but uses a non-parametric distribution instead of a Gaussian distribution.

$$\nabla H_i = k * \frac{d}{d\theta_i}(Density^{-1}(\theta_i)) \qquad (5)$$

To increase the accuracy of the solution, the joint angle data were divided into groups based on end effector position. The end effector space was divided into evenly spaced increments, along the x, y, and z axes of the reference frame. This creates a number of discrete sets of data, equal to the cube of the number of increments along each axis, that were used to create the probability density distributions. The selection of the increment used was based on the position of the hands (end effectors) at each instance of the trial. The associated probability density distribution for that increment was then used to find the gradient vector. This accuracy of the probability density gradient projection was tested for increments from 1 to 20 along each axis. The probability function serves partially as a joint limit function by restricting movement outside of observed joint angles. This ensured that a stable solution was reached. The ranges of observed joint angles were always within theoretical anatomical joint limits. Therefore, the probability density function imposed a greater constraint on motion than a joint limit constraint would.

RMS error was calculated by finding the root of the mean of the square of the difference between the predicted joint angles and the recorded joint angles.

$$\boldsymbol{RMSerror} = \sqrt{\frac{\sum(\boldsymbol{\theta_{MA}} - \boldsymbol{\theta_X})^2}{\boldsymbol{N}}} \qquad (6)$$

The errors were then evaluated for each subject and the number of subjects who's data was included in the creation of the density function was varied from 1 to 10, as shown in TABLE II. This allows the evaluation of the sensitivity of the method to included and excluded data to be determined. If the method is found to be insensitive to the amount of included data it is called robust.

TABLE II. Data distribution for robustness testing

	Robustness Test Number										
	1	2	3	4	5	6	7	8	9	10	
Excluded	C01	C01 - C02	C01- C03	C01 - C04	C01 - C05	C01 - C06	C01- C07	C01 - C08	C01 - C09	C01 - C10	Included
	C02 - C10	C03 - C10	C04 - C10	C05 - C10	C06 - C10	C07 - C10	C08 - C10	C09 - C10	C10	-	

V. Results

An example of the joint angle density function is shown in Figure 2, and the associated inverse density and gradient function are shown in Figure 3.

Figure 2. Density function for torso extension (joint 1)

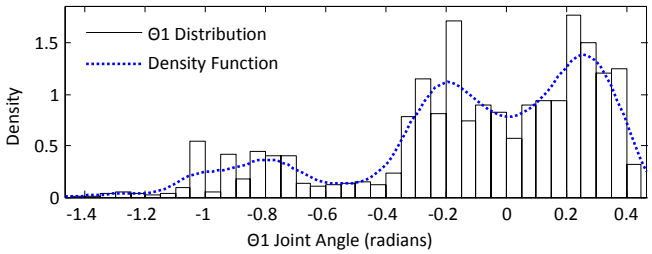

Figure 3. Inverse density and gradient function for torso extension (joint 1)

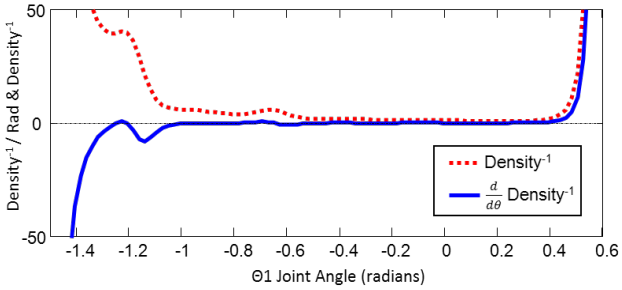

The LN method produced an average RMS error of 11.1° (±1.5°). This method exhibits increasing accuracy as the amount of workspace division increases, as shown in Figure 4. In the extreme case, this would end in each point of the workspace being assigned a specific joint angle distribution, if sufficient data were available. For the tested increments, the average RMS error for the GP method ranged from 7.7° (±1.0°) for 1 increment to 3.7° (±0.4°) for 20 increments. A Wilcoxon two-sided rank sum test was performed in Matlab between the subject RMS error of the GP and LN methods found that the difference between methods was significant for all increments, ($p < 0.001$).

Figure 4. GP accuracy vs. division of end effector space

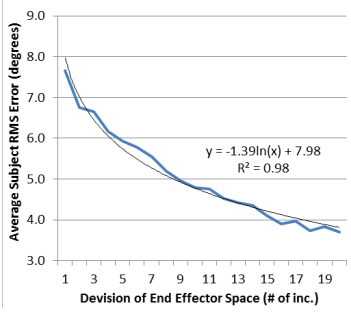

The robustness of the GP method was very low for greater number of increments (*inc.*), the error for subjects whose data was included in the density function set was low, while the error for persons in the excluded data set was high. The addition of more data to included data set has little effect on the error of either sets. As the number of increments decreases, the robustness of the GP increases. Using a logarithmic regression on each data set, *inc*=19 will likely never converge, *inc*=10 will likely converge with 162 subjects (at an estimated average error of 6.6°), and with *inc*=5 will likely converge with 23 subjects (at an estimated average error of 7.5°). The coefficient of determination (r^2) was used to evaluate the confidence in the regression. The fit was poor ($r^2 < 0.8$) for the subject data included in the density function, and good ($0.80 < r^2 < 0.99$) for the subject data excluded from the density function. The average RMS joint angle error for each data set of the *inc*=5 increment level robustness tests are given in Figure 5.

Figure 5. Robustness of the GP method with 5^3 workspace increments (*inc*=5), for subjects included and excluded from the density function.

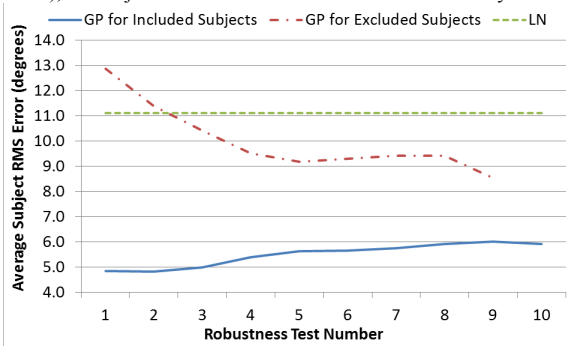

VI. Discussion

This paper presented an analysis of the probability density gradient projection (GP) method for predicting human upper body inverse kinematics. The impact of adding additional increments was greatest when the number of increments was low, and decreases as the number grows. With the limited data available for this study, increasing the number of increments also increases the number of end effector sets where no data were available. In these positions, the GP method behaves the same as the least norm solution. From this analysis, the GP methods with fewer increments may be more appropriate because they are more robust while they still provide a reasonable prediction of subject motion. Also, the GP method with a low numbers of increments is still significantly better than the LN. At this point it is clear that additional data is needed to verify the performance of the GP method, since extrapolation of existing data is not a reliable method. Further development of methods and testing with recorded human motion will likely improve the accuracy and reliability of the GP method for predicting human motion. The gradient projection of the RHBM's null-space is appealing because it allows for the optimization of a wide variety of constraints, yet it is difficult because it requires tuning of the rate of convergence of the function to ensure stability. Overall, this method presents an acceptable solution to human-model inverse kinematics. Visual inspection of joint angle error when viewing the predicted pose appears good. This may be in part because the errors of the GP tend to be higher for joints that have high variation between subjects, and therefore do not appear unnatural when variation occurs. In this context, the performance of the GP method relative to the LN appears to be much better than suggested by the improvement in the RMS errors presented here. Development of additional method for evaluating the human likeness of predicted motions could also be used to further verify this and other methods.

References

[1] S. L. Carey, M. J. Highsmith, M. E. Maitland, and R. V. Dubey, "Compensatory movements of transradial prosthesis users during common tasks," *Clin Biomech (Bristol, Avon),* vol. 23, pp. 1128-35, Nov 2008.

[2] D. Lura, R. Dubey, S. Carey, and M. Highsmith, "Simulated Compensatory Motion of Transradial Prostheses," in *ASME International Mechanical Engineering Congress & Exposition (IMECE)*, Boston, Massachusetts, 2008.

[3] P. H. Chang, "A Closed-Form Solution for Inverse Kinematics of Robot Manipulators with Redundancy," *Ieee Journal of Robotics and Automation,* vol. 3, pp. 393-403, Oct 1987.

[4] S. Khadem and R. Dubey, "A Global redundant robot control scheme for obstacle avoidance," in *IEEE Southeast Conference*, Knoxville, TN, 1988, pp. 397-402.

[5] Y. Nakamura, *Advanced Robotics: Redundancy and Optimization*, 1st ed. Boston, MA, USA: Addison-Wesley Longman Publishing Co., Inc. , 1990.

[6] S. McGhee, T. F. Chan, R. Dubey, and R. Kress, "Probability-based weighting of performance criteria for a redundant manipulator," in *IEEE International Conference on Robotics and Automation (ICRA)*, San Diego, CA, 1994, pp. 1887-1894.

[7] D. Lura, S. Carey, R. Dubey, and M. Highsmith, "Robotic model for simulating upper body movement," in *International Conference on Robotics and Biomimetics (ROBIO)*, Bangkok, 2009, pp. 1135-1139.

[8] D. Lura, S. Carey, M. Highsmith, and R. Dubey, "Robot kinematics based model to predict compensatory motion of transradial prosthesis while performing bilateral tasks," in *International Conference on Robotics and Automation (ICRA)*, 2009, pp. 3104-3109.

[9] K. Abdel-Malek, J. Yang, Z. Mi, V. C. Patel, and K. Nebel, "Human upper body motion prediction," presented at the ASM Conference on Applied Simulation and Modeling, Rhodes, Greece, 2004.

[10] Z. Mi, J. Yang, and K. Abdel-Malek, "Optimization-based posture prediction for human upper body," *Robotica,* vol. 27, pp. 607–620, 2009.

[11] M. Troncossi, C. Borghi, M. Chiossi, A. Davalli, and V. Parenti-Castelli, "Development of a prosthesis shoulder mechanism for upper limb amputees: application of an original design methodology to optimize functionality and wearability," *Med Biol Eng Comput,* vol. 47, pp. 523-31, May 2009.

[12] E. B. Torres and D. Zipser, "Reaching to grasp with a multi-jointed arm. I. Computational model," *Journal of neurophysiology,* vol. 88, p. 2355, 2002.

[13] P. K. Artemiadis, P. T. Katsiaris, and K. J. Kyriakopoulos, "A biomimetic approach to inverse kinematics for a redundant robot arm," *Autonomous Robots,* vol. 29, pp. 293-308, 2010.

[14] A. A. Ali and A. H. Miry, "Human Arm Inverse Kinematic Solution Based Geometric Relations and Optimization Algorithm," *International Journal of Robotics and Automation (IJRA),* vol. 2, p. 245, 2011.

[15] C. Schönauer, "SKELETAL STRUCTURE GENERATION FOR OPTICAL MOTION CAPTURE," Institute for Software Technologies and Interactive Systems, Vienna University of Technology, 2007.

[16] D. Lura, S. Carey, and R. Dubey, "Validation of Functional Methods for Calculating the Shoulder Joint Center Using 3D Motion," presented at the ASME International Mechanical Engineering Congress and Exposition (IMECE), Vancouver, Canada, 2010.

[17] D. Lura, S. Carey, and R. Dubey, "Automatic Generation of a Subject Specific Upper Body Model From Motion Analysis Data," in *Proceeding of the ASME 2011 International Mechanical Engineering Congress & Exposition (IMECE2011)*, Denver, Colorado, USA, 2011.

[18] J. J. Craig, *Introduction to robotics: mechanics and control*, 2nd ed.: Addison-Wesley Longman Publishing Co., Inc., 1989.